

# BEAMS3D Neutral Beam Injection Model $\ddagger$

Matthew McMillan

Samuel A. Lazerson

**Abstract.** With the advent of applied 3D fields in Tokamaks and modern high performance stellarators, a need has arisen to address non-axisymmetric effects on neutral beam heating and fueling. We report on the development of a fully 3D neutral beam injection (NBI) model, BEAMS3D, which addresses this need by coupling 3D equilibria to a guiding center code capable of modeling neutral and charged particle trajectories across the separatrix and into the plasma core. Ionization, neutralization, charge-exchange, viscous slowing down, and pitch angle scattering are modeled with the ADAS atomic physics database [1]. Elementary benchmark calculations are presented to verify the collisionless particle orbits, neutral beam injection model, frictional drag, and pitch angle scattering effects. A calculation of neutral beam heating in the NCSX device is performed, highlighting the capability of the code to handle 3D magnetic fields.

*Keywords:* Fusion, Magnetics, Diagnostics, Equilibria, Reconstruction

Submitted to: *Plasma Phys. Control. Fusion*

$\ddagger$  Notice: This manuscript has been authored by Princeton University under Contract Number DE-AC02-09CH11466 with the U.S. Department of Energy. The United States Government retains and the publisher, by accepting the article for publication, acknowledges that the United States Government retains a non-exclusive, paid-up, irrevocable, world-wide license to publish or reproduce the published form of this manuscript, or allow others to do so, for United States Government purposes.

## 1. Introduction

Modern toroidal confinement fusion devices use significant auxiliary neutral beam heating systems that must be accounted for in magnetohydrodynamic (MHD) equilibrium calculations. Direct measurement of fast ion pressure profiles is difficult [2], and often requires forward modeling of fast ion physics. Fast ions are modeled on a background equilibrium magnetic field, and the results applied to recompute the field. While some devices are nominally axisymmetric (Tokamaks), and well validated codes such as NUBEAM exist to provide 2D fast ion models, all devices exhibit 3D field structure whether applied (resonant magnetic perturbations, stellarators, and error field compensation) or intrinsic (long-lived helical modes, helical axis states, and error fields). This motivates the development of neutral beam and fast ion codes capable of handling fully 3D field structure.

In this paper we report on the development of a fully 3D model for neutral beam injection and fast ion deposition, orbit, and thermalization. The BEAMS3D code models charged particle gyro-center motions in 3D fields and is parallelized over particle trajectories. Equilibrium fields are calculated using the VMEC code [3] coupled to virtual casing routines for external fields [4]. Particle deposition is calculated from neutral particle trajectories including the physical effects of charge-exchange and recombination, pitch angle scattering, and viscous slowing down. Realistic aperture models allow full neutral beam injection calculations. This provides a robust tool for evaluating neutral beam effects in various devices with 3D field structure.

This paper consists of three principle sections, followed by a concluding discussion of future work. We first give a detailed description of the computational model assumed in BEAMS3D. The next section discusses and verifies the elementary physical effects, which are collisionless vacuum orbits, ionization/neutralization reactions, viscous slowing down, and pitch angle scattering. The third section demonstrates the capabilities of the code by modeling the injection and thermalization of particles in a finite beta NCSX equilibrium [5].

## 2. Computational Model

The BEAMS3D code models charged particle orbits in 3D fields with the guiding center approximation for charged particles. The magnetic field is represented by splines over a cylindrical grid allowing for an accurate representation of the field geometry in 3D. The field is constructed from vacuum and equilibrium fields. A virtual casing principle is invoked for calculation of plasma fields outside the equilibrium domain. The beam injection model includes focal point, direction, aperture, and energy parameters to accurately model the straight-line neutral trajectories. Local plasma parameters along a neutral trajectory are used to calculate the expected flight time before ionizing, at which point pitch angle and parallel velocity are computed. The guiding center motions of the charged particles are governed by drift kinetic equations, and various collisional and

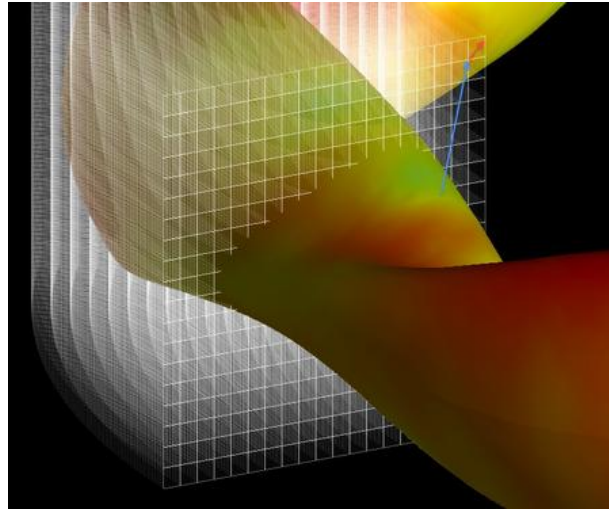


**Figure 1.** Depiction of the BEAMS3D cylindrical grid with 3D equilibrium. Fields are initialized with a combination of vacuum fields, equilibrium fields, and plasma response as calculated through a virtual casing principle.

recombination physics are included through the ADAS library to reproduce physical particle orbit effects. At present, these effects comprise electron and ion impact ionization and charge exchange ionization, re-neutralization of fast ions (charge exchange loss), viscous slowing down, recapture of partially slowed neutrals, and pitch angle scattering. The code is parallelized over the particle orbits using MPI architecture and output data is available in the HDF5 data format [6].

### 2.1. Neutral Beam Injection and Gyro-Center Motion

The neutral beam model defines the straight-line trajectory for neutral particle injection. The neutral beam parameters include: focal point (back of the beam), direction (any other point along the desired beam line), beam divergence, distance from focal point to aperture, aperture size (given as a circle radius; the code is easily modified to assume a square aperture or any other shape), a number of particles to launch from the focal point, and finally the mean energy of the neutral particles. The particles are launched from the focal point towards the aperture plane with velocity distributions according to a Gaussian from a single user-defined mean energy (standard deviation assumed to be one tenth of the mean). The velocity directions are taken from a 2D Gaussian in the aperture plane, with mean at the center of the aperture, and standard deviation calculated from the beam divergence. Then the particles are tested to determine whether they are blocked by the aperture, and the initial conditions for those particles that exit the aperture are used to initialize the particle trajectories starting at the focal point. These particle trajectories will be tracked until time runs out or until they exit the simulation domain.

Neutral particles are followed along straight-line trajectories (Fig. 2), and ionization is governed by statistics. At the start of its trajectory each particle is assigned a random

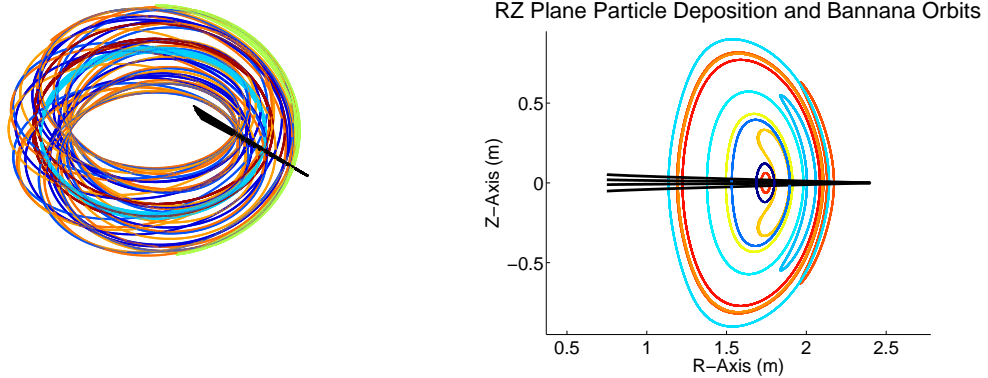


**Figure 2.** A 3D (left) and R-Z projection (right) of a simulation of particle injection into a D-shaped Tokamak plasma. Black lines indicate neutral particle trajectories while colored lines depict gyro center motion in the plasma. Both trapped and passing orbits are present.

number  $\xi_{rand}$  in the range  $(0, 1)$  representing a random probability in the cumulative ionization probability distribution; 1 represents immediate ionization, 0 ionization after infinite time. Each particle is also given a current location in that distribution,  $\xi^*$ , initialized to 1. At each time step along the trajectory,  $\xi^*$  is reduced according to

$$\xi^* = \xi^* e^{-\frac{dt}{\tau_{fl}}},$$

where the expected time of flight for the particle is

$$\tau_{fl} = \left[ \sum_j n_j \langle \sigma_j v_{rel} \rangle \right]^{-1}.$$

Here  $j$  is the species of interest and averages are over the ionization reaction cross sections (e.g. electron and ion impact, charge exchange). When  $\xi^*$  falls below  $\xi_{rand}$  the particle is considered to have changed charge state and ionized. The process for neutralization of hot-ions (recombination) is nearly identical, with  $\tau_{fl}$  the general expected flight time before *switching* state. Any reaction cross sections available in the ADAS database may be included in the summation.

The ionization location is used to calculate the initial conditions for the charged particle guiding center trajectory. The initial position of the guiding center is taken to be perpendicular to the local magnetic field where the neutral ionized (one gyro-radius away). This is consistent with the idea that the particle is now orbiting in a helix with central curve one gyroradius from the particle. For neutralization reactions, the reverse process is applied, but with the phase of the particle in its gyromotion chosen at random. It should be noted that while designed to model neutral beams, the code may also be initialized with charged particle positions, velocities, and pitch angles. This feature was used extensively in verifying the gyrocenter evolution solver in the code.

Once ionized, the particle gyrocenters are evolved according to the guiding center drift kinetic equations:

$$\begin{aligned}\frac{d\vec{R}}{dt} &= \frac{\hat{b}}{qB} \times \left( \mu \nabla B + \frac{mv_{\parallel}^2}{B} (\hat{b} \cdot \nabla) \vec{B} \right) + v_{\parallel} \hat{b} \\ \frac{dv_{\parallel}}{dt} &= -\frac{\mu}{m} \hat{b} \cdot (\nabla B)\end{aligned}$$

where  $\hat{b} = \frac{\vec{B}}{B}$ ,  $\mu = \frac{1}{2} \frac{mv_{\perp}^2}{B}$  is the magnetic moment, and  $v_{\parallel} = \frac{d\vec{R}}{dt} \cdot \hat{b}(\vec{R})$  is the component of velocity parallel to  $\vec{B}$ . Measurement of  $E_{\parallel}$  in stellarators has only recently become available and is open to some speculation, so for simplicity we follow Fowler et al. [11, eqns. 16-20] and omit the term. Integration options include LSODE [7], Adams' method (NAG D02CJF) [8], and a 4th order Runge-Kutta solver [9]. This paper exclusively uses the NAG algorithm. Particles are pushed with a maximum time step (between calls to the physics routines) which is predetermined to keep the physical step size below a user-defined limit.

For each particle, BEAMS3D records  $(R, \phi, z)$  coordinates, Boozer  $(s, u, v)$  coordinates,  $v_{\parallel}, \mu$ , and a neutralization logical along the particle trajectory. These can be used to compute energy and momentum deposition in post simulation data analysis, as well as many other quantities of interest. To improve statistics in Monte-Carlo simulations, particles are also assigned a positive real number *weight*. For example, convergence might be difficult for particles in the edges of the beam distribution, so one might increase the number of particles launched there and decrease their weight such that the weighted distribution remains Gaussian.

## 2.2. Viscous Fast Ion Slowing (Friction Drag)

Viscous slowing, or friction drag, is a primary contributor in the thermalization process. BEAMS3D simulates the effect by reducing parallel velocity and magnetic moment (i.e., gyration component) at each time step for which the solution is provided to the physics routine. The appropriate rate equation can be derived from the Fokker-Planck distribution function, with a term for the ion-impact contribution and one for the electron-impact contribution. We direct the reader to Callen [10], Fowler [11], or Rosenbluth [12] for details and cite the result:

$$\frac{\partial \langle v \rangle}{\partial t} = -\frac{v}{\tau_s} - \frac{v_c^3}{\tau_s v^2} = -\frac{v}{\tau_s} \left( 1 + \frac{v_c^3}{v^3} \right). \quad (1)$$

The first term represents drag on electrons, predominant for high velocity fast ions, and the second term represents drag on background ions, predominant for lower velocity (nearly thermalized) fast ions. Here  $v$  is the *speed*,  $\tau_s$  is the Spitzer ion-electron momentum exchange time [10], and  $v_c$  is the critical velocity associated with the critical energy at which the velocity reduction transitions from nearly exponential (drag on electrons) to significantly steeper (drag on ions). (For this work we assume the absolute speed; in future versions one could introduce a term to account for plasma velocity.)

Given a particle location in the plasma, the physics routine in the code is called, which uses the local  $T_e$  and  $n_e$  to compute  $\tau_s$  and  $v_c$  according to the formulae:

$$\tau_s = \frac{m_i}{m_e} \frac{(4\pi\epsilon_0)^2}{4\sqrt{2\pi}} \frac{3m_e^{1/2}T_e^{3/2}}{n_e Z_i^2 e^4 \ln \Lambda}, \quad (2)$$

$$v_c = \left[ \frac{3\sqrt{\pi}}{4} \frac{m_e}{m_i} \right]^{1/3} v_{T_e}, \quad (3)$$

where

$$v_{T_e} = \sqrt{\frac{2T_e}{m_e}}, \quad \ln \Lambda = \begin{cases} \frac{23 - \ln(n_e^{1/2} Z T_e^{-3/2})}{24 - \ln(n_e^{1/2} T_e^{-1})} & T_e < 10Z^2 eV \\ & \\ & T_e > 10Z^2 eV, \end{cases} \quad (4)$$

$m_i$ ,  $m_e$  are the ion and electron masses, and all other parameters are standard. Now the speed is

$$v = \sqrt{v_{\parallel}^2 + v_{\perp}^2} = \sqrt{v_{\parallel}^2 + \frac{2\mu B}{m}} \quad (5)$$

where all terms on the right are available to the physics routine. This yields a differential reduction in speed that naturally splits into parallel and moment components:

$$\tilde{v} = v + \Delta v = v - \frac{v}{\tau_s} \left( 1 + \frac{v_c^3}{v^3} \right) \Delta t \quad (6)$$

$$v_{\parallel} \mapsto \frac{\tilde{v}}{v} v_{\parallel} \quad (7)$$

$$\mu \mapsto \left( \frac{\tilde{v}}{v} \right)^2 \mu. \quad (8)$$

These trajectory modifications are applied every time the physics routine is called.

### 2.3. Pitch-Angle Scattering

The last physics effect we address is the pitch angle scattering. Our method closely follows that of Fowler et al. [11] and we refer the reader there for more details. At each solution time step, the physics routine takes a new pitch angle from a distribution:

$$P(\zeta) = \frac{1}{\sqrt{2\pi}\sigma} \exp \left( -\frac{(\zeta - \langle \zeta \rangle)^2}{2\sigma^2} \right), \quad (9)$$

where the variance  $\sigma^2$  is taken from moments of the pitch-angle term of the Fokker-Planck equation. The formulae are:

$$\sigma^2 = \frac{2v_s \Delta t}{v^3} (1 - \zeta_0^2), \quad (10)$$

$$\langle \zeta \rangle = \zeta_0 \left( 1 - \frac{2v_s \Delta t}{v^3} \right), \quad (11)$$

$$v_s = \frac{v_c^3}{2\tau_s} \frac{m_i}{m_f} \frac{\langle Z \rangle}{[Z]}, \quad (12)$$

$$\langle Z \rangle = \frac{\sum_j n_j Z_j^2}{\sum_j n_j Z_j}, \quad (13)$$

$$[Z] = \frac{\sum_j n_j Z_j^2 (m_i/m_j)}{\sum_j n_j Z_f}, \quad (14)$$

where  $\zeta_0$  is the pitch angle of the particle prior to scattering, and  $\zeta$  is the new, scattered, pitch angle. The last two definitions ( $\langle Z \rangle$ ,  $[Z]$ ) are taken from Fowler, Smith, et al. [13]. In this paper, we assume pure hydrogen plasma and fast ions, so these terms are both identically 1 and  $v_s$  reduces to  $v_s = v_c^3/2\tau_s$ .

### 3. Verification and Simulation

#### 3.1. Collisionless Particle Orbits

We tested the particle following code block to ensure that collisionless particle orbits fulfill expectations. To verify this part of the code, a set of test particles was launched, starting as ions in the equilibrium, from a range of radial locations and with a range of energies and pitch angles. A large aspect-ratio circular cross-section Tokamak equilibrium field was used, and the resulting banana orbits were compared with those anticipated from an analytic derivation. The banana width formula may be written

$$\Delta r = 2 \left( \frac{R}{r} \right)^{1/2} q\rho,$$

where  $R$  is the major radius,  $r$  is the radius from toroidal axis to banana,  $q$  is the safety factor, and  $\rho$  is the gyroradius [14]. We show that the banana width scales linearly with  $\rho$ .

Figure 3 shows a plot of the particle trajectories in the cylindrical coordinates used by the ODE solver (so here X is  $R$  and Y is  $z$ ). All particles start on the inner arc and bounce back and forth between  $\theta = \pi/2$  and  $\theta = -\pi/2$ . The different outer edges (shown as different colors on the expanded graph) show the outermost radial positions of the particles. The banana widths are measured from this outermost position to the inner edge on the  $z = 0$  line. The results are shown in Figure 4 as a log-log plot of the banana width,  $\Delta r$ , vs. perpendicular velocity,  $v_\perp$  (i.e., energy). The slope of 1 indicates the scaling of the banana widths agrees with analytic estimates. The low residual in the fit of the data corroborates the assertion that charged particle gyrocenters are being modeled correctly.

#### 3.2. Viscous Fast Ion Slowing (Friction Drag)

In an effort to verify the frictional drag effect in the code, a group of particles was launched from inside the equilibrium of a D-shaped Tokamak. The decay in total energy over time was compared to an artificial solution of the drag equations. The differential

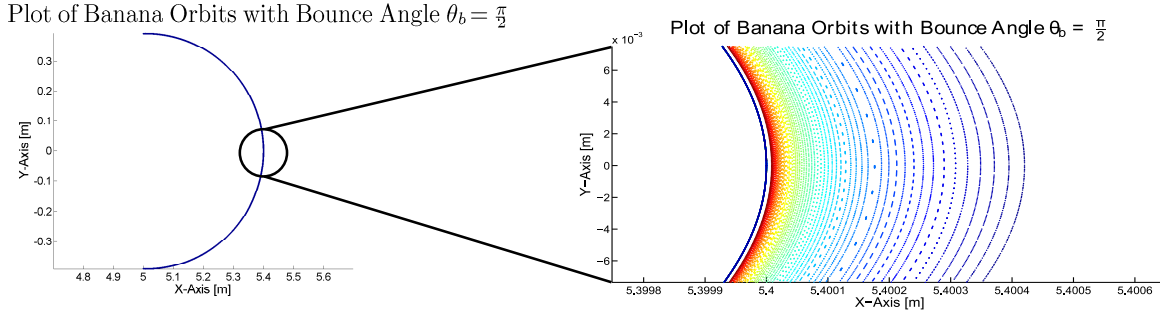


**Figure 3.** Banana orbits for constant pitch, 2.5 order range in energy. A large aspect ratio (10) circular cross-section Tokamak field is used.

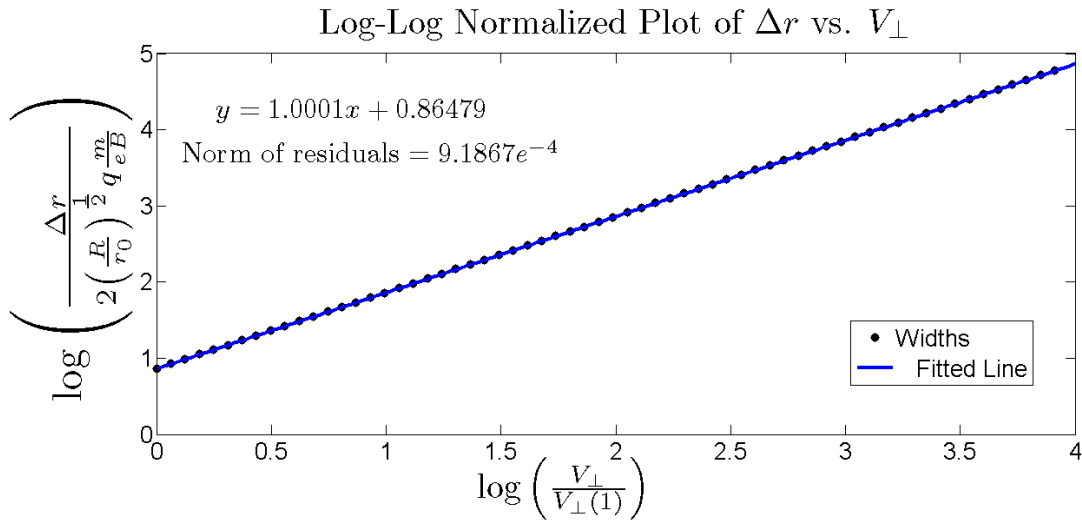


**Figure 4.** Normalized log-log plot of banana width versus  $v_{\perp}$ , showing a linear relationship, consistent with the analytic result for this  $\vec{B}$  field.

equation for speed was directly solved for each particle by using plasma parameters from the flux surface containing that particle, and the corresponding energy decay compared to that produced by BEAMS3D.

Figure 5 shows this comparison. The solid lines are the energy decay plots provided by the model, and the adjacent dashed lines are the artificial solutions produced by solving the drag equations entirely outside of the model context. Note that the pitch-angle scattering effect is disabled. The good agreement between the two indicates that the slowing effect has been implemented correctly. Now the drag rate for slow particles is predominantly determined by the ratio  $v_c^3/v^2$ , so for a normal fluctuation of  $v_c$  about its mean (corresponding to any particle in the actual equilibrium field), the slowing effect on the particle is skewed towards that of high  $v_c$  (more slowing). Thus we consistently see a slight lag in the artificial trajectories. This effect has been confirmed in more detail; high moment (or high pitch, hence high drift in flux surface) particles diverge more from the artificial solution than do low moment (low drift) particles, and always

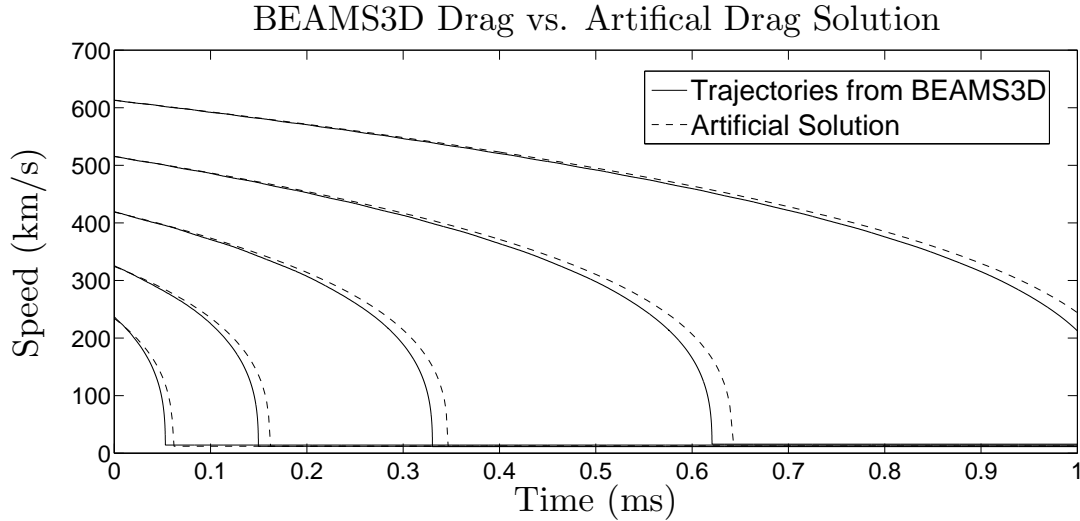


**Figure 5.** Plot of ion speeds, comparing trajectories of BEAMS3D to artificial solutions of the friction drag equation.

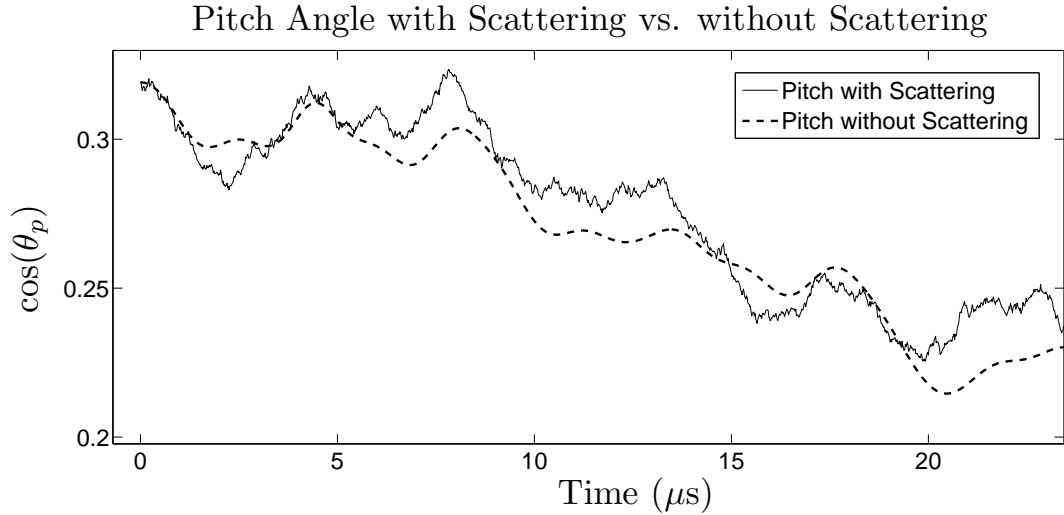


**Figure 6.** Plot of pitch angles, contrasting the pitch angles of a particle with versus without pitch angle scattering.

by more drag.

### 3.3. Pitch-Angle Scattering

The effect of pitch angle scattering is demonstrated in Figure 6 for two particles. The dashed path depicts the pitch angle of one particle launched in an NCSX equilibrium with the effects of pitch angle scattering and viscous drag turned off. The solid curve represents the same particle in the same situation, except the pitch angle scattering effect is turned on. Notice that aside from the scattering noise, they agree for early

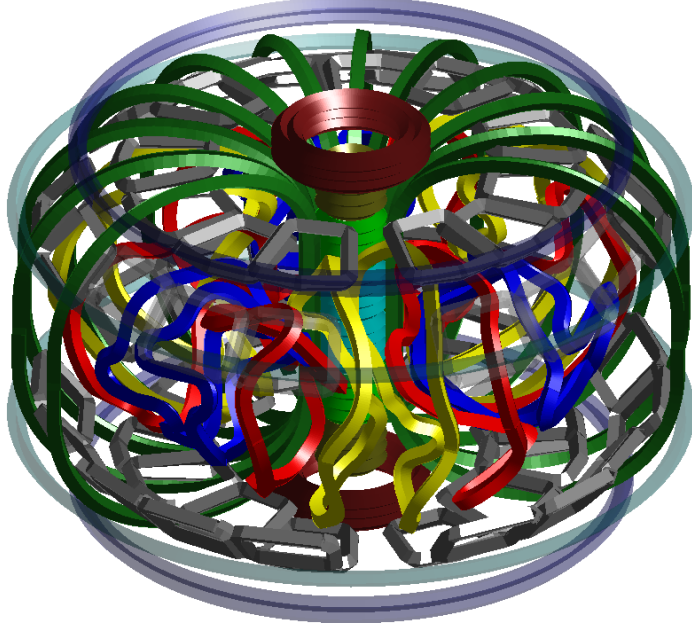


**Figure 7.** The NCSX coil set used for the calculation. The modular stellarator coils are depicted in red, yellow, and blue, while the vertical field coils have been made transparent for clarity. Some of the green TF coils have been removed for clarity as well. Coil thicknesses not to scale.

times. As time progresses, the global effect of scattering increases, causing significant change in the particle orbit.

### 3.4. NCSX Neutral Beam System

The advantages of the BEAMS3D code include its general representation of the magnetic field and its interface to VMEC 3D MHD equilibria. The cylindrical grid allows any toroidal magnetic field configuration to be represented, as long as a lookup function is provided which returns cylindrical  $\vec{B}$  given cylindrical position.

The code has been interfaced to VMEC allowing a demonstration of this capability using an NCSX equilibrium. The coil set for NCSX is shown in Figure 7. This coil set was used to compute an equilibrium with free boundary, finite plasma beta, and finite toroidal current density. It is important to note that the guiding center model may not be entirely applicable in the NCSX device, but does provide an approximation to a full orbit code.

The magnetic field on background gridpoints within the equilibrium domain are drawn from the NCSX equilibrium, and vacuum fields outside the VMEC equilibrium domain are computed by a Biot-Savart integration over the NCSX coil set [15]. A virtual casing principle is used to calculate the plasma response in this external region. Thus charged particles may be followed both inside and outside the VMEC equilibrium domain, all the way to the first wall structures. In this paper they were followed well

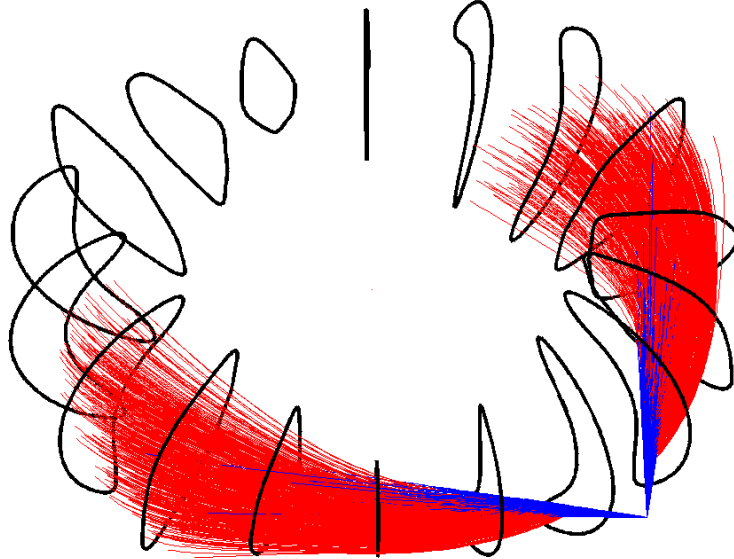


**Figure 8.** Depiction of neutral beam injection and particle ionization in the NCSX device. The two neutral beams (blue straight lines) were modeled with  $\sim 1000$  particles injected from a common origin in two directions. The trajectories of the charged particles (red) are plotted against the VMEC boundary for the equilibrium (solid black).

beyond the first wall structures.

The neutral beam details for the NCSX device are not finalized, so a trial set of tangential neutral beams was simulated [16]. A set of approximately 1000 particles was injected into the plasma, allowing the collection of rough particle statistics. Simulations could be scaled in practice up to a processor for every particle, but here 64 processors were used. Time steps were under a microsecond for particle following, ODE integration accuracy was  $10^{-10}$ , and the simulation took approximately 2 hours.

Figure 8 shows the neutral particles entering the plasma, ionizing, and being confined in the equilibrium. The neutral particle paths are calculated by the BEAM3D code as described in Section 2.1. The code uses local plasma densities and temperatures to adjust the remaining flight time for each neutral particle. Tangential injection results in nearly all particles ionizing before leaving the equilibrium as neutrals. The resulting population of  $\sim 1000$  charged particles then begin to orbit the device. In this simulation all particles that left the surface defined by the first wall soon hit the edge of the simulation domain and were considered lost and thus not included in the following analysis.

The effect of the slowing down reactions on the beam distribution function are shown in Figure 9. The peak parallel velocities decrease as the particles move through the plasma. The two beam directions result in a distribution function with distinct

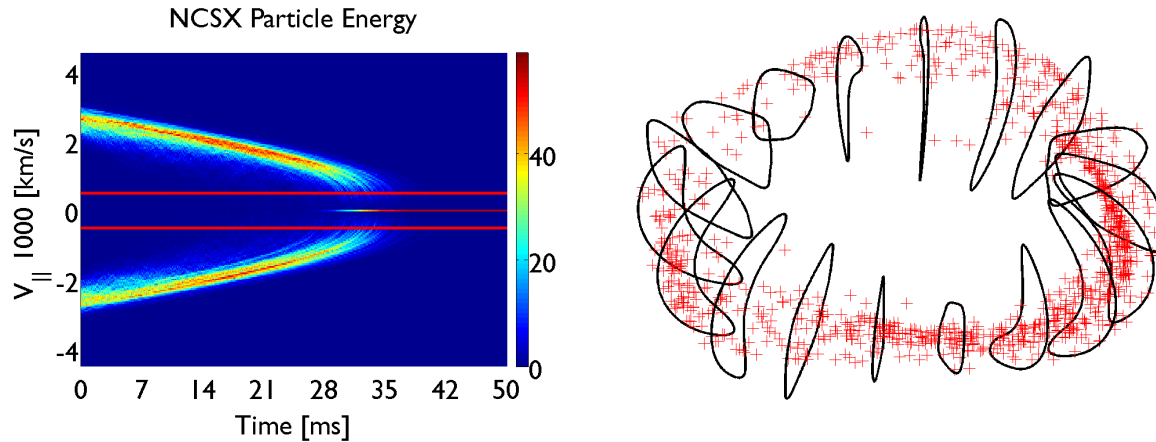


**Figure 9.** Evolution of the parallel energy for  $\sim 1000$  particles injected into the NCSX equilibrium (left) and location where they thermalized in the plasma (right). Red lines indicate the energy at which particles have slowed to  $1.5 \times$  the ambient ion energy. Particles followed beyond this energy tend to circulate at very low velocity. The color scale indicates the number of particles per keV energy bin.

parallel and anti-parallel components at  $t = 0$ . The red lines represent the velocity corresponding to  $\sim 1.5 \times$  the maximum local ion temperature in the plasma.

Particles are considered thermalized below this energy; the code continued to follow them past this and they all rapidly approached zero. The plot indicates that most particles have thermalized by  $t = 35$  ms. The effect of friction on the beam ions is clear, with energies decaying in time. Note that the final state of nearly all particles is not truly zero, but rather a low energy anti-parallel motion. This is probably an artifact of the way the slowing reactions are handled in the code, and suggests that in the future a cutoff might be used to terminate orbit following for thermalized particles.

#### 4. Conclusion

The BEAMS3D code provides researchers with a tool to evaluate 3D equilibrium effects on fast particle orbits and neutral particle injection. It supports the physics necessary to model fast ions in an MHD equilibrium, including deposition, charge exchange, scattering, and thermalization. The guiding center approximation is used to find particle trajectories, jumping a gyroradius step on each ionization or neutralization. The collisionless particle orbit banana widths have been tested, and the appropriate relationships with energy and radius found. The beam injection and deposition models have been implemented. Energy loss from viscous drag has been tested against an artificial solution to the drag equation, and pitch angle scattering has been implemented and verified as well. It should be noted that while other codes can follow particles inside the equilibrium domain, this code can follow particles across the boundaries of such a plasma domain.

Future work includes benchmarking against measurements of fast ion particle

distributions in real devices for which model solutions are known. As no unique benchmarks exist for codes such as BEAMS3D, the authors hope to develop a set of test problems which may serve as benchmarks for all neutral beam codes. Key to this would be the ability of these test problems to gauge the limits of a given model without comparison to other codes. Validation of BEAMS3D against experimental data is also planned. Specifically, the BEAMS3D code can begin to address neutral beam injection measurements in the LHD as well as W7-X. Further improvements would also include incorporation of more particle-plasma interactions, interfacing to more sophisticated equilibrium codes, and adding terms to account for radial (parallel) electric field and plasma speed. Although the 3D splines are demanding in terms of memory, the possibility of GPU computation of particle orbit calculations has also been discussed.

## Acknowledgments

The authors would like to thank M. Gorelenkova for her valuable guidance regarding the implementation of the ADAS libraries and discussions regarding NUBEAM. We would also like to extend thanks to R. White for his useful discussion of collisionless particle orbits. Finally, we acknowledge the Summer Undergraduate Laboratory Internship (SULI) program funded by the DOE Office of Workforce Development for Teachers and Students.

- [1] H P Summers, M G O'Mullane, A D Whiteford, N R Badnell, and S D Loch. ADAS: Atomic data, modelling and analysis for fusion. In *ATOMIC AND MOLECULAR DATA AND THEIR APPLICATIONS: 5th International Conference on Atomic and Molecular Data and Their Applications (ICAMDATA)*, pages 239–248. AIP.
- [2] M Salewski, B Geiger, A S Jacobsen, M García-Muñoz, W W Heidbrink, S B Korsholm, F Leipold, J Madsen, D Moseev, S K Nielsen, J Rasmussen, M Stejner, G Tardini, M Weiland, and the ASDEX Upgrade Team. Measurement of a 2D fast-ion velocity distribution function by tomographic inversion of fast-ion D-alpha spectra. *Nuclear Fusion*, 54(2):023005, January 2014.
- [3] Steven P Hirshman and J C Whitson. Steepest-descent moment method for three-dimensional magnetohydrodynamic equilibria. *Physics of Fluids*, 26(1):3553–3568, December 1983.
- [4] Samuel Lazerson. The virtual-casing principle for 3D toroidal systems. *Plasma Physics and Controlled Fusion*, 54(12):122002, November 2012.
- [5] M C Zarnstorff, L A Berry, A B Brooks, E Fredrickson, G Y Fu, Steven P Hirshman, Stuart R Hudson, L P Ku, Edward A Lazarus, David R Mikkelsen, D Monticello, G H Neilson, N Pomphrey, Allan H Reiman, D Spong, D Strickler, Allen H Boozer, W A Cooper, R J Goldston, R Hatcher, M Isaev, C Kessel, J Lewandowski, J F Lyon, Peter Merkel, H Mynick, B E Nelson, C Nuehrenberg, M Redi, W Reiersen, P Rutherford, R Sanchez, J Schmidt, and R B White. Physics of the compact advanced stellarator NCSX. *Plasma Physics and Controlled Fusion*, 43(12A):A237–A249, November 2001.
- [6] The HDF Group. *HDF5 Reference Manual*, 1.8.1 edition, November 2011.
- [7] A. C. Hindmarsh. ODEPACK, A Systematized Collection of ODE Solvers , R. S. Stepleman et al. (eds.), North-Holland, Amsterdam, (vol. 1 of ), pp. 55-64. *IMACS Transactions on Scientific Computation*, 1:55–64, 1983.
- [8] James Murray Watt and G Hall. *Modern numerical methods for ordinary differential equations*. Clarendon Press Oxford, 1976.

- [9] D Sarafyan. Improved sixth-order runge-kutta formulas and approximate continuous solution of ordinary differential equations. *Journal of Mathematical Analysis and Applications*, 40(2):436–445, 1972.
- [10] JD Callen. Fundamentals of plasma physics. *Lecture Notes, University of Wisconsin, Madison*, 2003.
- [11] R H Fowler, R N MORRIS, J A Rome, and K HANATANI. Neutral Beam Injection Benchmark Studies for Stellarators/Heliotrons. *Nuclear Fusion*, 30(6):997–1010, June 1990.
- [12] Marshall N Rosenbluth, William M MacDonald, and David L Judd. Fokker-Planck Equation for an Inverse-Square Force. *Phys.Rev.*, 107:1–6, 1957.
- [13] R H Fowler, J Smith, and J A Rome. FIFPC - a Fast Ion Fokker-Planck Code. *Computer Physics Communications*, 13(5):323–340, January 1978.
- [14] Roscoe B White. *The Theory of Toroidally Confined Plasmas*. Imperial College Press, London, 2 edition, January 2001.
- [15] James D Hanson and Steven P Hirshman. Compact expressions for the Biot–Savart fields of a filamentary segment. *Physics of Plasmas*, 9(10):4410, 2002.
- [16] H W Kugel, D Spong, R Majeski, and M C Zarnstorff. NCSX plasma heating methods. *Fusion Science and Technology*, 51(2):203–217, February 2007.